Megjelenési adatok:

Journal of Solid State Electrochemistry **17** (2013) 3075-3081.
DOI 10.1007/s10008-013-2158-4
(Beküldve: 2013. április 30. / Javított változat: 2013. június 10. / Elfogadva: 2013. június 12.)

A systematic approach to the impedance of surface layers with mixed conductivity forming on electrodes

László Péter

Institute for Solid State Physics and Optics, Wigner Research Centre for Physics, Hungarian Academy of Sciences

1525 Budapest, P. O. Box 49, Hungary

Phone: +361-392-2222, ext 3614; Fax: +361-392-2215; E-mail: peter.laszlo@wigner.mta.hu

Abstract – Electrode impedance can be evaluated on the basis of the electrode reaction kinetics in many systems, even for complicated electrode reactions. However, when a surface layer is present on the electrode surface, the theoretically well-established impedance model of the electrode reaction is often completed with phenomenological equivalent circuit elements in order to achieve the number of time constants as derived from the electrode impedance spectra measured In these cases, the meaning of the phenomenological equivalent circuit elements are often unclear, though the presence of these elements is helpful to describe the system throughout the frequency domain used for the measurement. In the present work, an attempt will be shown to separate the effect of the electronic and ionic charge transfer in a surface layer and to identify the appropriate equivalent circuits. Examples are shown from the fields of lithium-ion batteries where a solid electrolyte interface as a surface layer is present at the negative electrode and the contribution of various charge carriers may be of importance.

1. Introduction

Electrochemical impedance spectroscopy (EIS) is a well-established technique to reveal mechanistic details of various electrode processes. EIS is a popular and convenient tool to identify the contribution of the charge transfer, the diffusion of the reactant, the adsorption of the reactants and/or the intermediates, and the intercalation of the ions. The above mentioned steps – or those that are indeed a part of the actual electrode process – together make the impedance of the electrode reaction (Z_{ER}). The impedance or admittance functions of many electrode reactions can be calculated with exact mathematical methods, even though it might not be possible to construct an equivalent circuit in all cases.

Besides the electrode reaction, the impedance measured for a particular electrode as a whole comprises additional circuit elements. Due to the electric double layer that builds up between the first-order and second-order conducting phases (that are mostly a metal and an electrolyte solution, respectively), the interface exhibits an inherent capacitive nature. This is represented in the electrode impedance with the so-called double layer capacitance (C_{DL}), which is connected parallel to the impedance of the electrode reaction, indicating the parallel ways of the current flow. A serial resistance element (that is called in most cases the solution resistance) must also be taken into account to evaluate the data measured. This element is unrelated to the electrode processes themselves but accounts for the cell geometry; namely, the non-infinitely close position of the potential reference point to the working electrode certainly leads to an ohmic drop. The solution resistance is a serial circuit element. The conventional representation of the equivalent circuit of an electrode reaction can be depicted with the circuit as shown in Figure 1a. When the impedance of the electrode reaction includes the charge transfer resistance and a diffusion (Warburg) impedance, it is known as the Randles circuit.

However, the above described treatment of the electrode impedance can be applied under special circumstances only. The most important criterion is that the electrolyte components accounting for the double layer behaviour have to be present in a large enough concentration (supporting electrolyte). Also, it should be provided that the double layer charge/discharge process is fully independent of both the electrode reaction and the specific adsorption on the electrode surface; i.e., the supporting electrolyte must be electrochemically incative. If this condition is not fulfilled, the equivalent circuit of the electrode process needs to be modified, and even a diffusion impedance element may have to be included if the species responsible for the capacitive processes are present in a small concentration only [1,

2]. In the case when the species taking part in the Faraday reaction are the same as those responsible for the double layer properties, the Warburg impedance is often connected in series with the ($C_{DL} \| R_{CT}$) branch. This is often the case when electrodes for lithium-ion batteries are studied, and the fit of the parameters by using such circuits are generally satisfactory [3-10]. Nevertheless, such circuits have not been theoretically established so far.

All features mentioned above hold for an electrode in which there is a direct contact between the electron-conducting and the single ion-conducting phase. This is a scheme in which the interface with capacitive properties can be unambiguously identified, and the resistance R_S can be connected serial with all other circuit elements. However, in many kinds of electrode the electron-conducting phase is covered with another solid layer and, hence, the interface where the Faraday reaction takes place is separated from the electrolyte solution. Two typical examples are shortly described below:

(i) When a corroding electrode is covered with a passive (and typically oxide-type) surface layer, the oxidation of the metal takes place at the metal/passive layer interface. The oxide layer may exhibit a mixed conductivity, and all possible interfaces may have their capacitive contribution to the overall electrode behaviour. Similarly, the surface layer can have a resistive contribution to the total electrode impedance.

(ii) On the negative (carbonaceous or Li) electrode of Li-ion batteries, an intermediate layer must form to provide the functionality of the electrode and to make it possible to intercalate Li in a reversible manner. This layer is generally called the solid-electrolyte interface (SEI) that is created by the first charge-discharge cycle of the cell and which also protects the electrolyte solution from any further decomposition.

The conduction mechanism of the surface layers on the electrodes is difficult to describe since they usually cannot be synthesized in bulk form. Nevertheless, the presence of an additional non-insulating solid layer at the electrode surface is known to increase the number of time constants in the alternating current behaviour of the electrode. Due to the insufficient knowledge on the conduction mechanism and the uncertainty in the involvement of such layers in the electrode process, a phenomenological approach is usually applied to account for the behaviour of these layers. Namely, a parallel RC sub-circuit is added to the theoretically established impedance related to the electrode reaction. The possible ways of adding this sub-circuit in order to account for the number of the time constants found experimentally are shown in Figs. 1b and 1c. Apparently, the circuit shown in Fig. 1b is widespread [11-13] but not exclusively used [14, 15] in the corrosion literature, while

researchers dealing with lithium-ion batteries favor the circuit shown in Fig. 1c [16-34] in an overwhelming majority. Another concept is applied by Lewandowski and coworkers [35,36] who prefer an R_{EL}–Z_W–{$C_{SEI} \| (R_{SEI} (C_{DL} \| R_{CT}))$} type equivalent circuit, which exhibits time constants in the same number as the circuits shown in Figs. 1b and 1c. It is difficult to judge the quality of the models since practically no paper reports on the impedance data fitted with more than a single model circuit; therefore, there is a great room for elucidation trials.

Although the quantitative description of the alternating current behaviour of the coated electrodes becomes satisfactory with the inclusion of one or even several [37-44] additional parallel RC sub-circuits, this may also give rise to some doubts concerning the relevance of the phenomenological approach:

(i) No processes are identified that give rise to the occurrence of an additional time constant in the overall electrode behaviour. Therefore, the fit values of the circuit elements added may miss any meaning; or, at least, these parameters cannot be connected to elemental processes.

(ii) It is doubtful with which other circuit elements the double layer capacitance is to be connected in parallel. Depending on the assumption on the location of the capacitive interface, the resistance of the surface layer must be taken into account, in connection with either the ionic or electrical transport in this layer.

In the following part, an attempt will be made to take into account the role of the surface layer in a theoretically correct manner.

2. Theoretical

Below, an electrode with a solid surface layer will be considered. In the surface layer, both ionic and electron transport will be allowed. The charge transfer caused by the ion motion (diffusion or migration) and the electron transport will be considered as independent and parallel conduction channels. In this model, two interfaces appear: one between the electrode metal and the solid surface layer and another between the surface layer and the electrolyte solution. Both interfaces are allowed to serve as a capacitive one. Therefore, the inner part of the surface layer may behave in a similar way as the electrolyte solution in a simple electrode; i.e., the charge accumulated at the metal surface is compensated by a diffuse ion cloud in the solid surface layer. At the same time, the outmost boundary of the solid surface layer is also capable to accumulate some extra charge, the compensation of which is provided by the ion redistribution in the Helmholtz layer of the solution, similarly to the

conventional solid electrodes. The charge transfer to both surfaces with capacitive properties is hindered by a respective resistance originating from either the ion or the electron transfer through the solid surface layer. The charge transfer between chemical species (i.e., the electrode reaction itself) is allowed to take place at a single boundary only. Hence, all possible kinds of electrochemical reactions occur at the boundary of the first-order conductor/SEI interface only. The schematic representation of the equivalent circuit of this layer structure is depicted in Figure 2 showing also both the geometric separation of the layers and the independent conduction channels.

The immediate consequence of the separation of the roles of the charge carriers is that the high-frequency limit of the real part of the impedance will be $R_{SOL}+(R_{SL,e}^{-1}+R_{SL,ion}^{-1})^{-1}$. Therefore, the high-frequency limit has a different meaning as compared to the case of a bare metal electrode when the resistance of the surface layer is substantial. Depending on the density and on the mobility of the charge carriers in the surface layer, either the electrical or ionic resistance of the surface layer may have a dominant contribution to the high-frequency impedance of the system. In any case, the high-frequency impedance is no longer a simple and meaningless parameter to be deduced from the total impedance.

It has to be noticed that the equivalent circuit shown in Figure 2 necessarily leads to a so-called “depressed semicircle behaviour” (referring to the Nyquist plot of the electrode impedance). As the frequency of the measurement decreases, the resistance in series to the impedance of the electrode process will become $R_{SOL}+R_{SL,ion}$, which is higher than the high-frequency limit of the real part of the impedance. Therefore, the high to medium-frequency part of the impedance is stretched along the real axis of the Nyquist plot, giving rise to a depressed semicircle. Although such depressed semicircles are often modeled with a constant phase element (CPE) replacing a capacitor in a regular equivalent circuit, the present approach draws the attention to the fact that the application of the CPE is often a phenomenological tool to describe a system quantitatively when our knowledge on the system is insufficient.

Although the complete quantitative analysis of the circuit shown in Fig. 2 is difficult, some trends can be clearly established. The present model can also be responsible for the occurrence of a new high-frequency semicircle in the Nyquist plot, similarly to the circuits shown in Figs. 1b and 1c. The two semicircles are in some cases well expressed, while the formation of a single depressed semicircle is also possible. A few simulated results are shown in Figure 3 where the impedance of the electrode reaction was taken to be a simple resistor

(R_{ER}) for sake of simplicity. It can be seen that, apart from extreme cases, the properties of the solid surface layer influence the high-frequency behavior of the system but lead to the same low-frequency behavior as for any other combination of the circuit elements related to the surface layer. At sufficiently low frequencies where the diffusion process can be noticed as the occurrence of a Warburg-type impedance, the circuit in Fig. 2 can be simplified and capacitors can be taken as elements with infinitely high impedance.

The occurrence of the semicircle related to the capacitance of the solution side of the surface layer is possible until the total impedance related to the electron transfer through the surface layer is lower or only comparably high to the other resistive elements. The separation of the two arcs in the Nyquist plot is related to the difference in the time constants of the processes related to the electron and ion transfer through the surface layer.

Figure 3c indicates that once the ionic conductivity of the surface layer is reduced, the entire impedance diagram shifts along the real axis. Although R_{SL} in the diagrams shown in Figs. 1b and 1c is introduced pronouncedly for the resistance of the surface layer, its change does not modify the high-frequency behavior, unlike the parameter $R_{SL,ion}$ in the circuit presented in Fig. 2.

Figure 4 shows the comparison of two impedance functions calculated with different equivalent circuits. Although the calculation of the exact equivalence conditions is not easy, it can be seen that the impedance functions calculated with different circuits correspond to each other at least at the same level that is accepted during the fit of experimental impedance functions.

3. Comparison with result for electrode covered with a solid electrolyte interface

SEI formation on the negative electrode of a lithium-ion battery is an important but badly understood process. On the surface of both carbon-type and metallic Li negative electrodes, the decomposition of the solvent results in an insoluble and presumably polymer-type layer that plays a crucial role in the functionality of the electrode. The formation of SEI can be followed by the excess charge needed for the first charging process.

Due to the lack of an ex-situ synthesis method, the properties of SEI cannot be studied independently of the electrode itself. The big majority of the impedance studies of the negative electrodes of Li batteries underpin that the number of time constants is larger than what is needed for the description of the metal deposition/dissolution (for Li anode) or

intercalation/de-intercalation (for carbon-type anode). Therefore, an ($C_{SL} \| R_{SL}$) subcircuit is added to the system for the mathematical description of the alternating current behavior. Although it is straightforward to elucidate the meaning of the resistive element added, the explanation of the capacitive element is rather troublesome. The complications are even worse when a constant phase element is needed for the description of the electrode behavior [4, 6-8, 10, 17, 18, 22, 26, 29-34, 45, 46]. No wonder that in many studies only the resistive elements obtained from the fit of the experimental impedance data are given [3, 6-9, 16, 21, 23-25, 28-30, 32-34, 36, 37, 43, 44, 46, 47], and the indication of all parameters fitted is rather scarce [18, 26, 31, 38, 40, 45]. The impedance of an electrode applied in lithium-ion batteries can seldom be fitted with the classical Randles circuit [48, 49] .

It is a common experience of the studies performed for both the negative electrodes of the Li ion batteries and the entire cells themselves that an increase of the high-frequency impedance is obtained upon cycling the system [10, 39-41, 45-47, 49-55]. Whichever popular model is used to describe this behavior (see, e.g., Figs. 1b and 1c), the high-frequency impedance should be invariant, unless something happens to the electrolyte. However, a large electrolyte excess is customarily used for the study of single electrodes and the solute content of a full Li-ion cell is presumably unchanged. Therefore, the positive shift of the impedance functions along the real axis of the Nyquist plot cannot be explained on the basis of the conventional models. The model proposed in this work and shown as the equivalent circuit in Fig. 2 offers a natural explanation for the rise of the high-frequency impedance because a conductivity decrease in SEI due to ageing leads to the enhancement of the real part of the impedance and does not require to include any capacitive element with an ill-defined meaning. This is well exemplified by the impedance diagrams shown in Fig. 3c.

4. Conclusion

The impedance of an electrode covered with a surface layer of mixed conductivity was considered. It was suggested that the electronic and ionic currents passed through the surface layer can be considered as parallel conduction channels. Sample impedance diagrams were shown that are in agreement with the impedance functions normally obtained for electrodes covered with a surface layer. In the model proposed, the capacitances of the inner and outmost boundary of the surface layer are naturally separated, and there is no need to connect an ($C \| R$) sub-circuit to either of the arm of the impedance function, eliminating the difficulty of the explanation of the meaning of the capacitance in this part of the equivalent circuit. It was

also noted that the blind correction of the "solution resistance" may lead to the loss of important data that are indicative of the behavior of the system studied. An overview of the literature of the solid electrolyte interface showed that the model proposed is worthwhile of testing for electrode impedance measurements and the change in the high-frequency limit of the impedance data measured may gain a natural explanation.

Acknowledgement

The author gratefully acknowledges Dr. Allen J. Bard for the postdoctoral research period spent in his lab in 1995-1997. This work was supported by the Hungarian Scientific Research Fund (OTKA) through grant # K 104 696.

References

1 Kerner Z, Pajkossy T (2002) Measurement of adsorption rates of anions on Au(111) electrodes by impedance spectroscopy. Electrochim Acta 47: 2055-2063

2 Pajkossy T, Kolb DM (2008) Anion-adsorption-related frequency-dependent double layer capacitance of the platinum-group metals in the double layer region. Electrochim Acta 53: 7403-7409

3 Yi J, Li XP, Hu SJ, Li WS, Zhou L, Xua MQ, Lei JF, Hao LS (2011) Preparation of hierarchical porous carbon and its rate performance as anode of lithium ion battery. J Power Sources 196: 6670-6675

4 Qiao YQ, Tu JP, Xiang JY, Wang XL, Mai YJ, Zhang D, Liu WL (2011) Effects of synthetic route on structure and electrochemical performance of $Li_3V_2(PO_4)_3$/C cathode materials. Electrochim Acta 56: 4139-4145

5 Wang C, Wang D, Wang Q, Chen H (2010) Fabrication and lithium storage performance of three-dimensional porous NiO as anode for lithium-ion battery. J Power Sources 195: 7432-7437

6 Zhao X, Tang X, Zhang L, Zhao M, Zhai J (2010) Effects of neodymium aliovalent substitution on the structure and electrochemical performance of $LiFePO_4$. Electrochim Acta 55: 5899-5904

7 Lewandowski A, Biegun M, Galinski M, Swiderska-Mocek A (2013) Kinetic analysis of Li|Li^+ interphase in an ionic liquid electrolyte. J Appl Electrochem 43: 367-374

8 Lin Y, Lin Y, Zhou T, Zhao G, Huang Y, Huang Z (2013) Enhanced electrochemical performances of $LiFePO_4$/C by surface modification with Sn nanoparticles. J Power Sources 226 : 20-26

9 Ma Z, Shao G, Wang G, Du J, Zhang Y (2013) Electrochemical performance of Mo-doped $LiFePO_4$/C composites prepared by two-step solid-state reaction. Ionics 19:437-443

10 Shi SJ, Tu JP, Tang YY, Zhang YQ, Liu XY, Wang XL, Gu CD (2013) Enhanced electrochemical performance of LiF-modified $LiNi_{1/3}Co_{1/3}Mn_{1/3}O_2$ cathode materials for Li-ion batteries. J Power Sources 225 : 338-346

11 Badawy WA, El-Rabiee M, Helal NH, Nady H (2012) The role of Ni in the surface stability of Cu–Al–Ni ternary alloys in sulfate–chloride solutions. Electrochim Acta 71: 50-57

12 Merl DK, Panjan P, Kovac J (2013) Corrosion and surface study of sputtered Al–W coatings with a range of tungsten contents. Corros Sci 69: 359-368

13 Rosalbino F, Maccio D, Scavino G, Saccone A (2012) In vitro corrosion behaviour of Ti–Nb–Sn shape memory alloys in Ringer's physiological solution. J Mater Sci: Mater Med 23:865–871

14 Pilbáth Z, Sziráki L (2008) The electrochemical reduction of oxygen on zinc corrosion films in alkaline solutions. Electrochim Acta 53: 3218-3230

15 Xu J, Wu X, Han EH (2012) The evolution of electrochemical behaviour and oxide film properties of 304 stainless steel in high temperature aqueous environment. ElectrochimActa 71: 219-226

16 An Y, Zuo P, Cheng X, Liao L, Yin G (2011) The effects of LiBOB additive for stable SEI formation of PP13TFSI-organic mixed electrolyte in lithium ion batteries. Electrochim Acta 56: 4841-4848

17 Kobayashi T, Seki S, Mita Y, Miyashiro H, Terada N, Kojima T (2010) AC impedance Analysis for 10 Ah-Class Lithium-ion Barreries. Electrochemistry 78: 416-419

18 Funabiki A, lnaba M, Ogumi Z, Yuasa S, Otsuli J, Tasaka A (1998) Impedance Study on the Electrochemical Lithium Intercalation into Natural Graphite Powder. J Electrochem Soc 145: 172-178

19 Funabiki A, Inaba M, Abe T, Ogumi Z (1999) Stage Transformation of Lithium-Graphite Intercalation Compounds Caused by Electrochemical Lithium Intercalation. J Electrochem Soc 146: 2443-2448

20 Wang Y, Wu M, Zhang WF (2008) Preparation and electrochemical characterization of TiO_2 nanowires as an electrode material for lithium-ion batteries. Electrochim Acta 53: 7863-7868

21 Guo P, Song H, Chen X, Ma L, Wang G, Wang F (2011) Effect of graphene nanosheet addition on the electrochemical performance of anode materials for lithium-ion batteries. Anal Chim Acta 688: 146-155

22 Zhou S, Wang D (2010) Unique Lithiation and Delithiation Processes of Nanostructured Metal Silicides. ACS Nano 4: 7014-7020

23 Dai C, Chen Z, Jin H, Hu X (2010) Synthesis and performance of $Li_3(V_{1-x}Mg_x)_2(PO_4)_3$ cathode materials. J Power Sources 195: 5775-5779

24 Dedryvere R, Foix D, Franger S, Patoux S, Daniel L, Gonbeau D (2010) Electrode/Electrolyte Interface Reactivity in High-Voltage Spinel $LiMn_{1.6}Ni_{0.4}O_4/Li_4Ti_5O_{12}$ Lithium-Ion Battery. J. Phys. Chem. C 114: 10999-11008

25 Hao X, Liu P, Zhang Z, Lai Y, Wang X, Li J, Liu Y (2010) Tetraethylammonium Tetrafluoroborate as Additive to Improve the Performance of $LiFePO_4$/Artificial Graphite Cells. Electrochem Solid-State Lett 13:A118-A120

26 Pramanik A, Ghanty C, Majumder SB (2010) Synthesis and electrochemical characterization of $xLi(Ni_{0.8}Co_{0.15}Mg_{0.05})O_2 - (1-x)Li[Li_{1/3}Mn_{2/3}]O_2$ $(0.0 < x < 1.0)$ cathodes for Li rechargeable batteries. Solid State Sci 12: 1797-1802

27 Rui XH, Yesibolati N, Li SR, Yuan CC, Chen CH (2011) Determination of the chemical diffusion coefficient of Li^+ in intercalation-type $Li_3V_2(PO_4)_3$ anode material. Solid St Ionics 187: 58-63

28 Wu XM, Chen S, Ma MY, Liu JB (2011) Synthesis of Co-coated lithium manganese oxide and its characterization as cathode for lithium ion battery. Ionics 17: 35-39

29 Yang T, Zhang N, Lang Y, Sun K (2011) Enhanced rate performance of carbon-coated $LiNi_{0.5}Mn_{1.5}O_4$ cathode material for lithium ion batteries. Electrochim Acta 56: 4058-4064

30 Zhang N, Yang T, Lang Y, Sun K (2011) A facile method to prepare hybrid $LiNi_{0.5}Mn_{1.5}O_4$/C with enhanced rate performance. J Alloys Compnd 509: 3783-3786

31 Lee SH, Jee SH, Lee KS, Nam SC, Yoon YS (2013) Enhanced cycling performance in heat-treated tin-based composite oxide anode for lithium-ion batteries. Electrochim Acta 87: 905-911

32 Lin Y, Lin Y, Zhou T, Zhao G, Huang Y, Yang Y, Huang Z (2013) Electrochemical performance of $LiFePO_4$/Si composites as cathode material for lithium ion batteries. Mater Chem Phys 138: 313-318

33 Nacimiento FJ, Lavela P, Tirado JL, Jiménez JM, Barreda D, Santamaría R (2013) ^{119}Sn Mössbauer spectroscopy analysis of Sn-Co-C composites prepared from a Fuel Oil Pyrolysis precursor as anodes for Li-ion batteries. Mater Chem Phys 138: 747-754

34 Tao HC, Huang M, Fan LZ, Qua X (2013) Effect of nitrogen on the electrochemical performance of core–shell structured Si/C nanocomposites as anode materials for Li-ion batteries. Electrochim Acta 89: 394-399

35 Lewandowski A, Kurc B, Stepniak I, Swiderska-Mocek A (2011) Properties of Li-graphite and $LiFePO_4$ electrodes in $LiPF_6$-sulfolane electrolyte. Electrochim Acta 56: 5972-5978

36 Lewandowski A, Swiderska-Mocek A, Waliszewski L (2013) Li^+ conducting polymer electrolyte based on ionic liquid for lithium and lithium-ion batteries. Electrochim Acta 92: 404-411

37 Hu Q, Osswald S, Daniel R, ZhuY, Wesel S, Ortiz L, Sadoway DR (2011) Graft copolymer-based lithium-ion battery for high-temperature operation. J Power Sources 196: 5604-5610

38 Moss PL, Au G, Plichta EJ, Zheng JP (2008) An Electrical Circuit for Modeling the Dynamic Response of Li-Ion Polymer Batteries. J Electrochem Soc 155: A986-A994

39 Moss PL, Au G, Plichta EJ, Zheng JP (2010) Study of Capacity Fade of Lithium-Ion Polymer Rechargeable Batteries with Continuous Cycling. J Electrochem Soc 157: A1-A7

40 Moss PL, Au G, Plichta EJ, Zheng JP (2009) Investigation of solid electrolyte interfacial layer development during continuous cycling using ac impedance spectra and micro-structural analysis. Journal of Power Sources 189: 66-71

41 Guo J, Sun A, Chen X, Wang C, Manivannan A (2011) Cyclability study of silicon-carbon composite anodes for lithium-ion batteries using electrochemical impedance spectroscopy. Electrochim Acta 56: 3981-3987

42 Levi MD, Aurbach D (1997) Simultaneous Measurements and Modeling of the Electrochemical Impedance and the Cyclic Voltammetric Characteristics of Graphite Electrodes Doped with Lithium. J Phys Chem B 101: 4630-4640

43 Hwang BJ, Chen CY, Cheng MY, Santhanam R, Ragavendran K (2010) Mechanism study of enhanced electrochemical performance of ZrO_2-coated $LiCoO_2$ in high voltage region. J Power Sources 195: 4255-4265

44 Schweikert N, Hofmann A, Schulz M, Scheuermann M, Boles ST, Hanemann T, Hahn H, Indris S (2013) Suppressed lithium dendrite growth in lithium batteries using ionic liquid electrolytes: Investigation by electrochemical impedance spectroscopy, scanning electron microscopy, and in situ ^{7}Li nuclear magnetic resonance spectroscopy. J Power Sources 228: 237-243

45 Dimesso L, Becker D, Spanheimer C, Jaegermann W (2012) Investigation of graphitic carbon foams/$LiNiPO_4$ composites. J Solid State Electrochem 16:3791-379

46 Li L, Li LY, Guo XD, Zhong BH, Chen YX, Tang Y (2013) Synthesis and electrochemical performance of sulfur–carbon composite cathode for lithium–sulfur batteries. J Solid State Electrochem 17:115-119

47 Zhang Y, Wang CY, Tang X (2011) Cycling degradation of an automotive $LiFePO_4$ lithium-ion battery. J Power Sources 196: 1513-1520

48 Tröltzsch U, Kanoun O, Tränkler HR (2006) Characterizing aging effects of lithium ion batteries by impedance spectroscopy. Electrochim Acta 51: 1664-1672

49 Ni J, Morishita M, Kawabe Y, Watada M, Takeichi N, Sakai T (2010) Hydrothermal preparation of $LiFePO_4$ nanocrystals mediated by organic acid. J Power Sources 195: 2877-2882

50 Hassoun J, Fernicola A, Navarra MA, Panero S, Scrosati B (2010) An advanced lithium-ion battery based on a nanostructured Sn-C anode and an electrochemically stable LiTFSi-Py_{24}TFSI ionic liquid electrolyte. J Power Sources 195: 574-579

51 Kim JH, Song SW, Hoang HV, Doh CH, Kim DW (2011) Study on the Cycling Performance of $Li_4Ti_5O_{12}$ Electrode in the Ionic Liquid Electrolytes Containing an Additive. Bull Korean Chem Soc 32: 105-108

52 Lewandowski A, Swiderska-Mocek A, Acznik I (2010) Properties of $LiMn_2O_4$ cathode in electrolyte based on N-methyl-N-propylpiperidinium bis(trifluoromethanesulfonyl)imide. Electrochim Acta 55: 1990-1994

53 Kim H, Lee JT, Yushin G (2013) High temperature stabilization of lithiumesulfur cells with carbon nanotube current collector. J Power Sources 226 : 256-265

54 Song H, Cao Z, Chen X, Lu H, Jia M, Zhang Z, Lai Y, Li J, Liu Y (2013) Capacity fade of $LiFePO_4$/graphite cell at elevated temperature. J Solid State Electrochem 17:599-605

55 Liao YH, Li XP, Fu CH, Xu R, Rao MM, Zhou L, Hu SJ, Li WS (2011) Performance improvement of polyethylene-supported poly(methyl methacrylate-vinyl acetate)-co-poly(ethylene glycol) diacrylate based gel polymer electrolyte by doping nano-Al_2O_3 . J Power Sources 196: 6723-6728

Fig. 1a

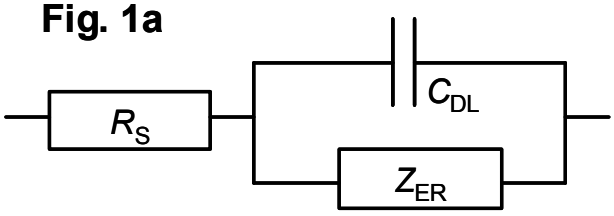

Fig. 1b

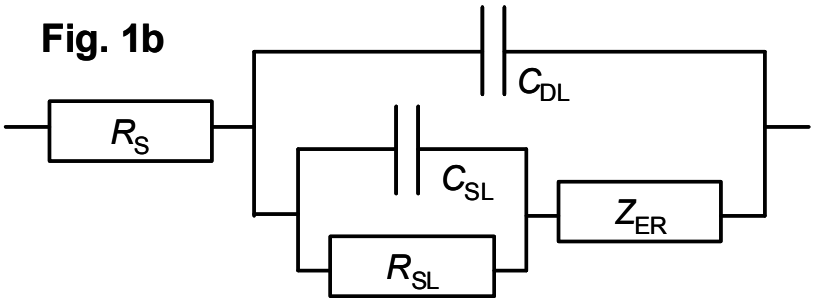

Fig. 1c

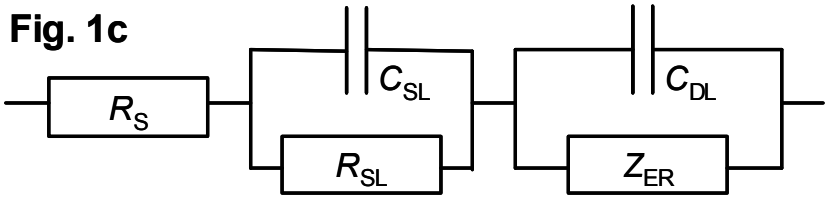

Figure 1 – 1a: The generally accepted equivalent circuit for an electrode reaction where no additional surface layer is present on the electrode surface. Figs. 1b and 1c: Frequently applied equivalent circuits for modeling electrode impedance where a solid surface layer is present on the electrode surface. SL denotes the surface layer and the other notations are the same as in the main text.

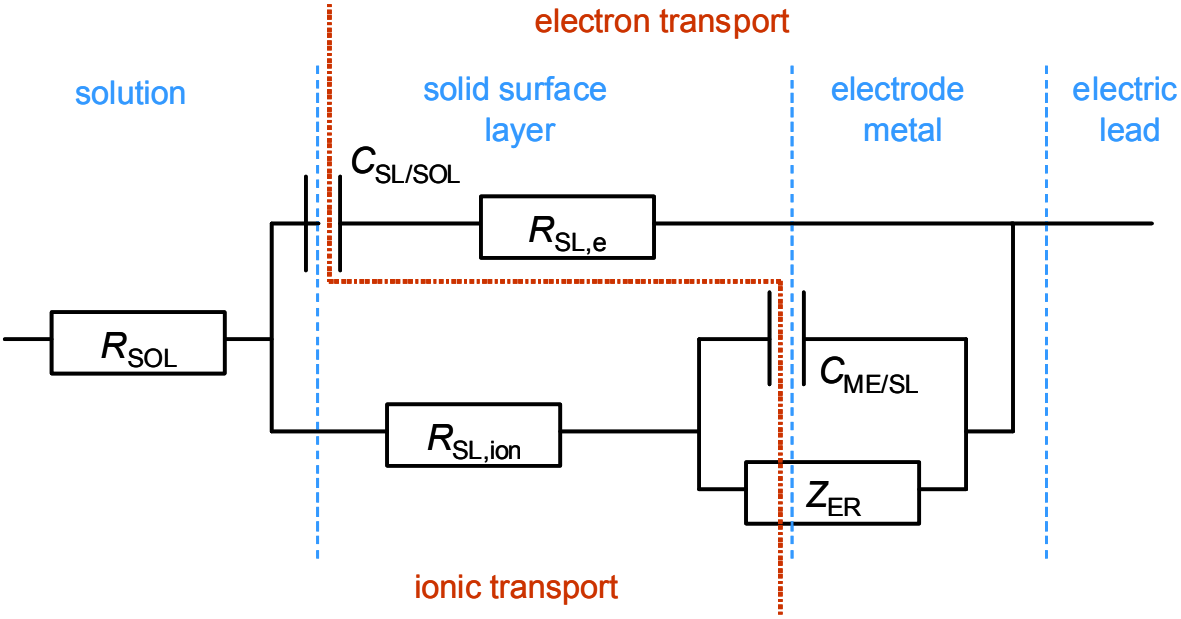

Figure 2 – The suggested equivalent circuit of an electrode covered with a solid surface layer exhibiting mixed electronic and ionic conductivity. Dashed lines indicate the phase boundaries and the thick dotted line separates the parts of the system where electrical and ionic means of charge transfer are dominant.

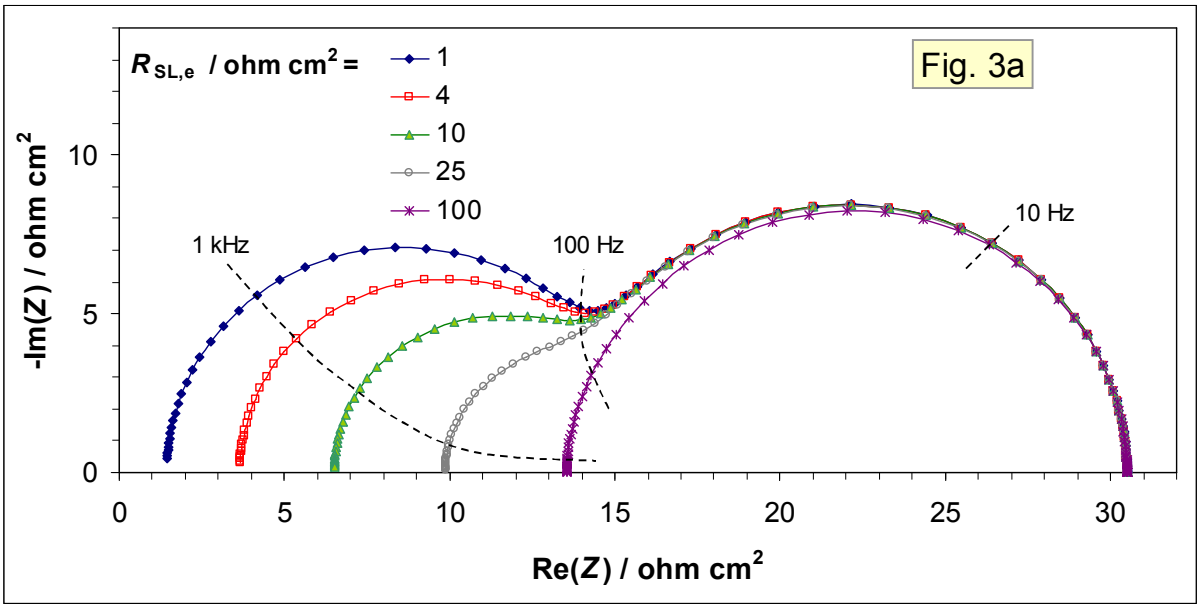
$R_{SL,e}$ / ohm cm^2 =
1
4
10
25
100
Fig. 3a
1 kHz
100 Hz
10 Hz
-Im(Z) / ohm cm^2
Re(Z) / ohm cm^2
0
5
10
15
20
25
30

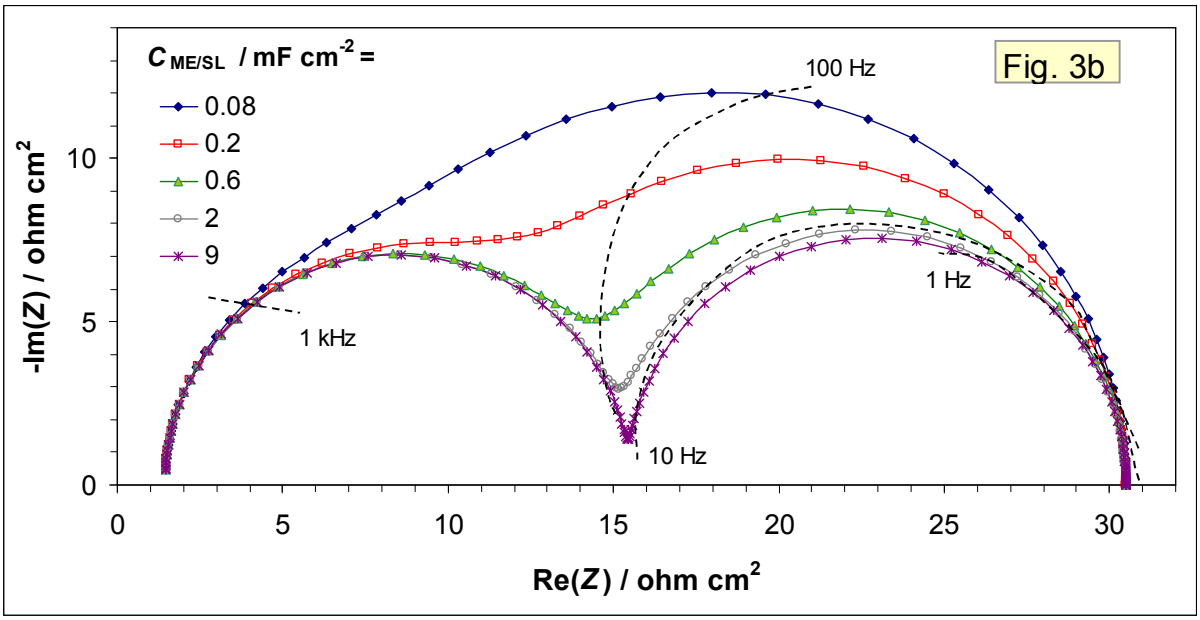
$C_{ME/SL}$ / mF cm^{-2} =
0.08
0.2
0.6
2
9
Fig. 3b
100 Hz
1 kHz
1 Hz
10 Hz
-Im(Z) / ohm cm^2
Re(Z) / ohm cm^2
0
5
10
15
20
25
30

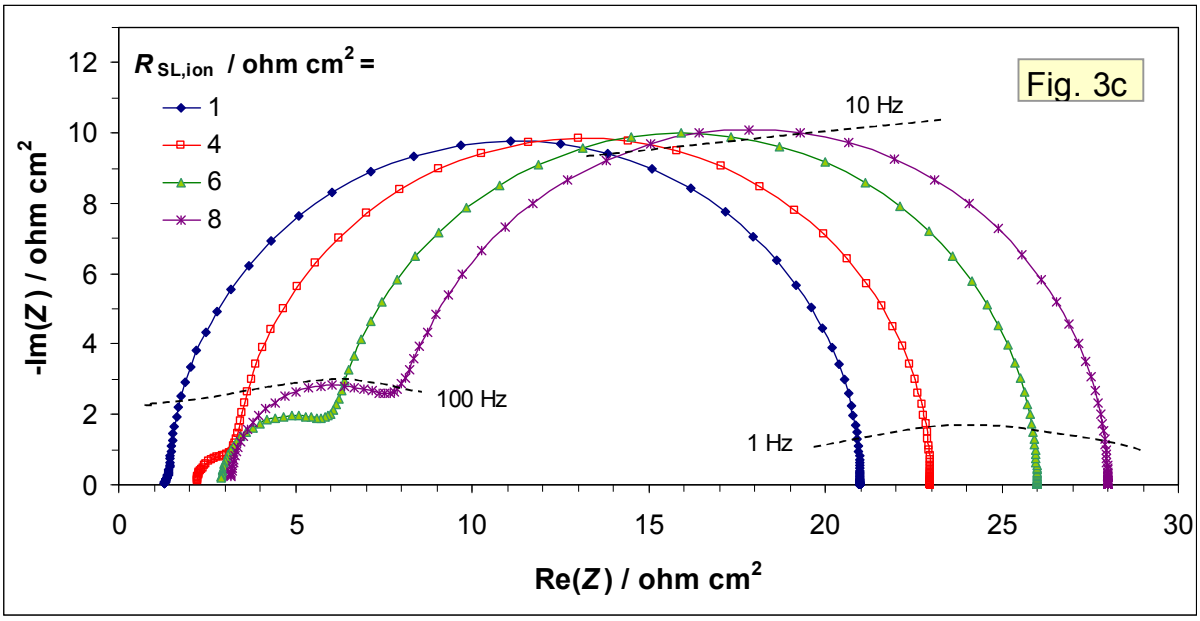

Figure 3 – Typical impedance diagrams obtained for the circuit shown in Figure 2 as a function of some parameters. R_{SOL} = 0.5 ohm cm^2 and $C_{SL/SOL}$ = 2x10^{-5} F cm^{-2} for all curves; dashed lines indicate the frequency of the perturbation.

a: $C_{ME/SL}$ = 6x10^{-4} F cm^{-2}, Z_{ER} = R_{ER} = 15 ohm cm^2, $R_{SL,ion}$= 15 ohm cm^2; $R_{SL,e}$ is indicated in the legend.

b: $R_{SL,e}$ = 1 ohm cm^2, Z_{ER} = R_{ER} = 15 ohm cm^2, $R_{SL,ion}$= 15 ohm cm^2; $C_{ME/SL}$ is indicated in the legend.

c: $C_{ME/SL}$ = 6x10^{-4} F cm^{-2}, Z_{ER} = R_{ER} = 19.5 ohm cm^2; $R_{SL,e}$ = 4 ohm cm^2, $R_{SL,ion}$ is indicated in the legend.

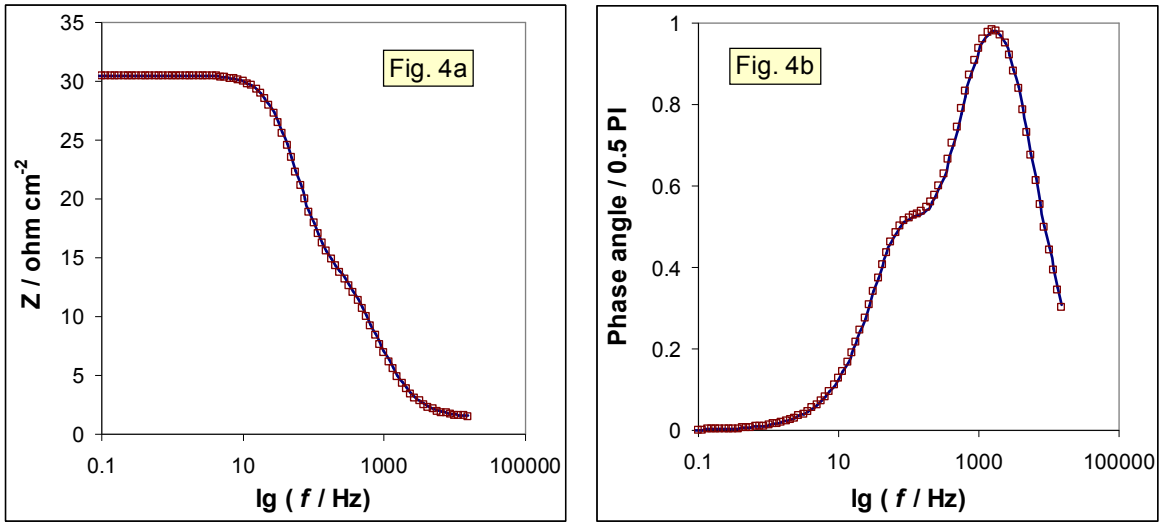

Figure 4 – Comparison of two impedance functions calculated with different equivalent circuits (Bode plot).

Symbols: Equivalent circuit as shown in Fig. 1c by using the following parameters: R_S = 1.452 ohm cm^2, R_{SL} = 17.908 ohm cm^2, C_{SL} = 0.185 mF cm^{-2}, Z_{ER} = R_{ER} = 11.14 ohm cm^2 and C_{DL} = 0.0252 mF cm^{-2}.

Line: Equivalent circuit shown in Fig. 2 by using the same parameters as in Fig. 3b, $C_{ME/SL}$ = 0.2 mF cm^{-2} (see the open squares in Fig. 3b).